

# A Bottom Fed Deployable Conical Log Spiral Antenna Design for CubeSat

Anthony J. Ernest, Youssef Tawk, Joseph Costantine, and Christos G. Christodoulou, *Fellow, IEEE*

**Abstract**—A conical log spiral antenna is presented with a new feeding scheme. This antenna is proposed for deployment on a CubeSat platform where the new feeding technique allows for easier antenna deployment. The antenna is composed of two arms that are wrapped around each other in a log-periodic manner. It is designed on top of a ground plane allowing its bottom feeding property. The feeding network is composed of quarter-wave-lengths transmission lines connected to a planar balun. The feeding network along with the balun provides the antenna with the appropriate impedance matching and phase shift between the two arms. The antenna is fabricated and tested. The measurement and simulation results show good agreement.

**Index Terms**—Balun, CubeSat, deployable antenna, helical antenna.

## I. INTRODUCTION

DEPLOYING antennas on a small satellite, such as a CubeSat, is a challenging process. The antenna's size especially within the ultra-high frequency (UHF) band rapidly approaches and exceeds the CubeSat standard dimensions of 10 cm × 10 cm × 10 cm [1]. Deployable antennas must be able to exhibit a larger aperture than their physical size while allowing a compact folding possibility for “easy” deployment once in space.

Several antenna concepts have been proposed for deployment on CubeSat. Reflector antennas for example are very popular since they achieve high gain (high sensitivity) or high directivity (a narrow beam and low side lobes) through aperture diameter sizing [2]. Other deployable antenna types include the 25-m class antenna discussed in [3].

Deployable planar antennas commonly used include reflect-arrays and synthetic aperture radar. Antenna concepts constructed with a folded hoop and six folded ribs to form a rigid backbone are also possible candidates as discussed in [4]. Neutrally elastic springs as well as bi-stable tape springs

Manuscript received October 28, 2013; revised April 27, 2014; accepted September 21, 2014. Date of publication November 05, 2014; date of current version December 31, 2014.

A. J. Ernest is with the Department of Electrical and Computer Engineering, University of New Mexico, Albuquerque, NM 87131 USA.

Y. Tawk, J. Costantine, and C. G. Christodoulou are with the Configurable Space Microsystems Innovation and Application Center (COSMIAC), The University of New Mexico, Albuquerque, NM 87131 USA (e-mail: christos@unm.edu).

Y. Tawk is with the Electrical and Computer Engineering Department, Notre Dame University, Louaize, Lebanon (e-mail: yatawk@ieee.org).

J. Costantine is with the Electrical and Computer Engineering Department, American University of Beirut, Beirut, Lebanon (e-mail: jcostantine@ieee.org).

Color versions of one or more of the figures in this paper are available online at <http://ieeexplore.ieee.org>.

Digital Object Identifier 10.1109/TAP.2014.2367539

constitute the basis for many antenna designs proposed for deployment on CubeSat platforms [5]–[8].

Helical antennas constitute one of the most popular choices for CubeSat deployment since they exhibit wide bandwidth, as well as circular polarization [1]. With a typical operation in the axial mode, helical antennas exhibit a varying half power beamwidth (HPBW) for different frequencies of the operating bandwidth.

The introduction of conical log spiral antennas in [9] has led to lower the back lobe radiation and the antenna physical size compared to a typical helical antenna. At the same time, the conical log spiral antenna preserves the same frequency independence behavior as the helical antenna. Therefore, a conical log spiral antenna is ideal for CubeSat deployment due to its frequency independent input matching, radiation pattern, and circular polarization.

One of the most important challenges in any antenna design for space communications applications is the feeding mechanism. Preserving a suitable input impedance match, while allowing a stable deployment mechanism, is a difficult task. The feeding of a conical log spiral antenna is typically achieved with an excitation at the top or apex of the conical structure with an appropriate feeding network [9]. This feeding mechanism adds difficulty to the deployment process in order to stabilize and position a feeding network at the apex of the antenna structure. In this paper, we show that a bottom fed conical log spiral antenna deployed on top of an optimized ground plane exhibits similar behavior to the top fed conical log spiral antenna and constitutes a suitable solution for CubeSat deployment.

This paper is divided as follows. In Section II, a comparison between the top fed and bottom fed conical log spiral antenna is provided. The proposed feeding network for the bottom fed antenna is shown in Section III. The fabricated prototype is detailed in Section IV and the comparison between the simulated and measured data is provided in Section V. Concluding remarks and future work constitute the last section of this paper.

## II. CONICAL LOG-SPIRAL ANTENNA

### A. Conical Log Spiral Antenna Design

The conical log spiral antenna fed at its top, where the apex of the cone is located, has a radiation pattern that is directed towards the vertex of the cone. This is explained due to the slow to fast wave nature of the non-active to active regions of the spiral arms, respectively, [10]. This transition leads to a backfire radiated pattern towards the conical vertex. Feeding the conical log spiral from the bottom of the antenna will result in the radiation pattern backfiring toward the base of the antenna and thus

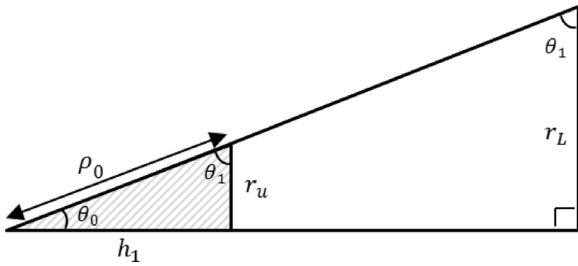


Fig. 1. Cross section of the conical log spiral antenna.

radiating towards the satellite. However, deploying the antenna with an optimized ground plane restores the radiation pattern direction towards the apex of the cone. This result in a similar behavior as the antenna fed at the top.

The upper and lower operating frequency band edges depend on the radii of the upper and lower circles constituting the conical structure, respectively. The antenna design dimensions are taken based on the study executed in [9]. The ratios of the upper and lower radii of the cone composing the conical log spiral affect the performance of the active region of the antenna. Thus, the radii dimensions of the upper and lower circles affect the near field as well as the far field radiation in addition to the bandwidth and half power beamwidth of the antenna itself. The radius of the upper circle ( $r_u$ ) and the one for the lower circle ( $r_L$ ), constituting the basis for the conical log spiral antenna design operating between 2 and 3.5 GHz, are derived from (1) [9]

$$\begin{aligned} r_u &= 0.067\lambda_u = 0.57 \text{ cm} \\ r_L &= 0.172\lambda_L = 2.58 \text{ cm}. \end{aligned} \quad (1)$$

The cross-section of the antenna cone can be seen in Fig. 1. Thus, the height of the antenna can be extrapolated from the conical angle and the radii of the base by using the trapezoid formula. If one wishes to compare the dimensions of the conical log spiral antenna to a typical helical antenna, one finds that the conical log spiral antenna is smaller in height compared to the helical antenna; however it has a larger diameter at the lower base.

The input impedance of the antenna is dependent on the width of the spiral arms as well as its conical angle. It was found that for very small and large widths, the input impedance is approximately  $320 \Omega$  and  $80 \Omega$ , respectively, [9]. The conical angle can also be increased or decreased to optimize the input impedance. However, any change in the conical angle has to preserve the conical topology of the antenna and cannot diminish the structure into a planar form. If the conical angle is increased until the arms are in a single plane, the theoretical impedance approaches that of an equiangular spiral antenna of  $60\pi$  or  $189 \Omega$ . As the governing equations do not take this facet into account, the impedance will have to be optimized during simulation modeling.

### B. Comparing Feeding Schemes

In this section, the two possible feeding mechanisms for the conical log spiral antenna are compared. The conventional feeding method is from the apex of the cone [11]. Both the top and bottom fed conical log spiral antennas are in a slow-wave

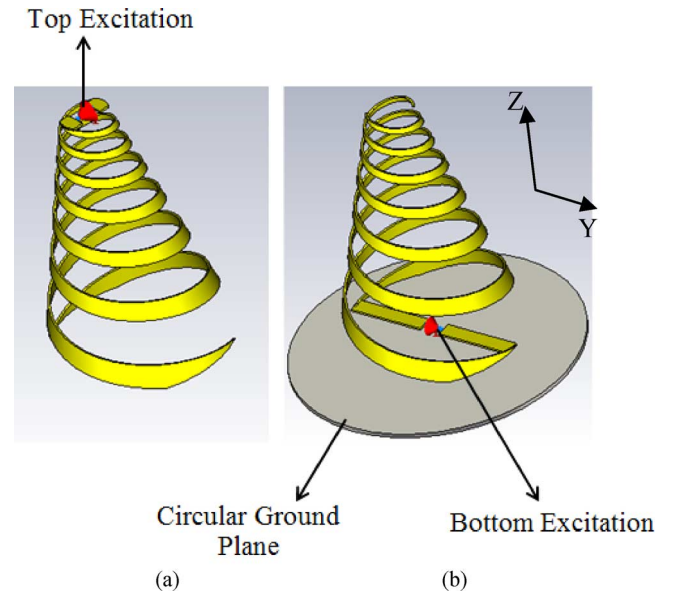


Fig. 2. (a) Top and (b) bottom fed conical log spiral antenna.

configuration within areas that are outside the “active region” of the antenna. Inside the active region the slow-wave nature changes into a fast-wave, where the wave changes directions and is backfired toward the vertex of the cone for the top fed or toward the base of the cone for the bottom fed scenario. The slow-wave area is made up of tightly bound surface waves, which continue as the propagation constant is increased. These tightly bound waves are coupled into a space wave travelling toward the vertex for the top fed or the base for the bottom fed and the propagation constant becomes complex. The complex propagation constant is the driving force that allows the traveling backfire wave that leads to the radiated power toward the apex or the base of the cone forming single directed beam [9].

Changing the location of the feed to the bottom of the antenna changes how the backfire radiation is produced. The active region should not be changed since the structure of the spiral arms have not changed. This means that the slow-wave nature changes into a fast-wave regardless of where the introduced antenna excitation is located. For the bottom fed antenna, the wave changes directions and is backfired away from apex of the cone and toward the feed. This will allow the radiated fields to be directed towards the CubeSat. To compensate for the reversed direction of the backfire, a ground plane below the antenna is proposed to provide an image that redirects the radiation towards the conical vertex.

First, a top fed antenna is simulated as shown in Fig. 2(a). This antenna is designed to operate between 2 and 3.5 GHz as detailed in the reflection coefficient plot of Fig. 3. The input port impedance is optimized and it is determined that a differential port impedance of approximately  $200 \Omega \pm 15 \Omega$  achieves the best matching for the target operating frequency.

To have a performance comparison between the feeding mechanisms for the top and bottom schemes, the bottom fed antenna is modeled, as shown in Fig. 2(b), on top of a circular ground plane. The same differential input impedance as the top fed antenna is used for the bottom fed case ( $200 \Omega$ ). Fig. 3 also

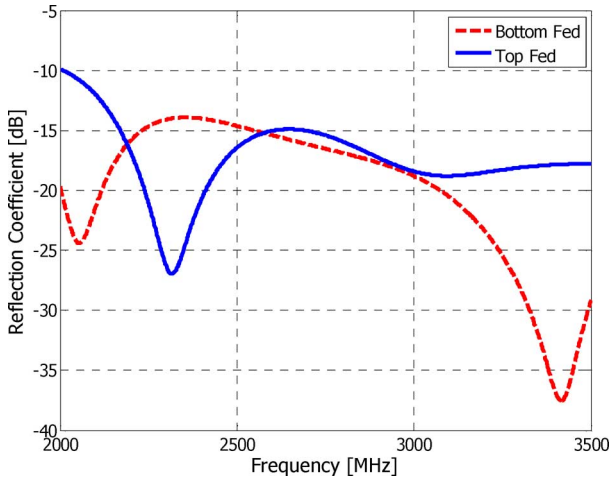


Fig. 3. Comparison of the reflection coefficient for both feeding schemes.

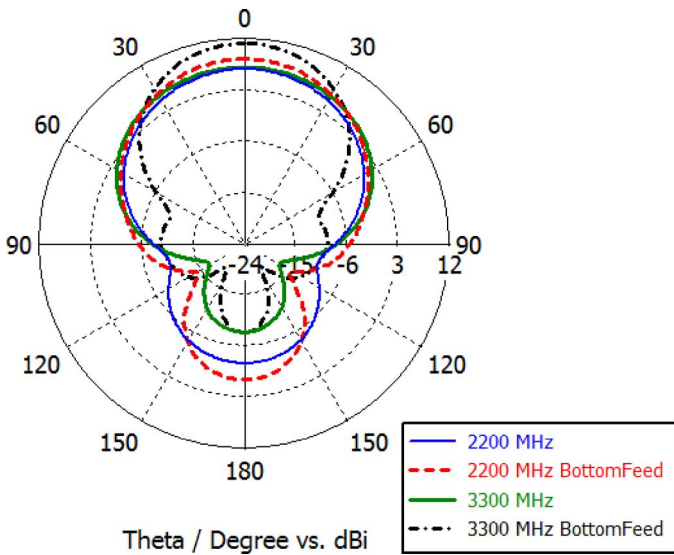


Fig. 4. Comparison of the polar cross section of the far field directivity patterns for both feeding schemes at 2.2 and 3.3 GHz.

shows the reflection coefficient for the bottom fed antenna. The same operating bandwidth is obtained.

Fig. 4 shows a polar cross section comparison of the 3-D radiated far field pattern of the two feeding configurations at the lower (2.2 GHz) and upper (3.3 GHz) band edges. The upper band edge has a higher directivity (11.2 dBi) resulting in a smaller HPBW, which is reduced from 90° to 50°. The directivity at the lower band edge is 8.4 dBi.

Investigating the electric field along the log-spiral, it can be seen that the beamwidth is reduced by the introduction of the ground plane. The ground plane size in function of wavelength is larger at the higher frequency bands. Thus, a larger effect on the higher frequency components is observed.

The 3-D far-field directivity for the bottom fed antenna is shown in Fig. 5 for  $f = 2.2$  and 3.3 GHz. It can be seen that the maximum radiation is directed towards the apex of the antenna cone and a wider beamwidth (lower directivity) is obtained at the lower frequencies.

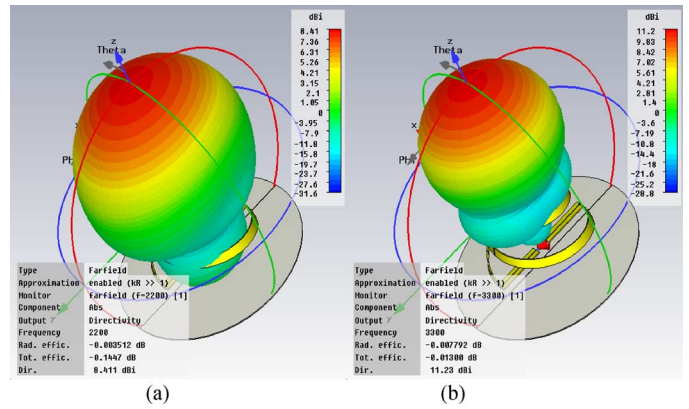


Fig. 5. Three-dimensional far-field directivity of the bottom fed conical log spiral antenna at (a) 2.2 and (b) 3.3 GHz.

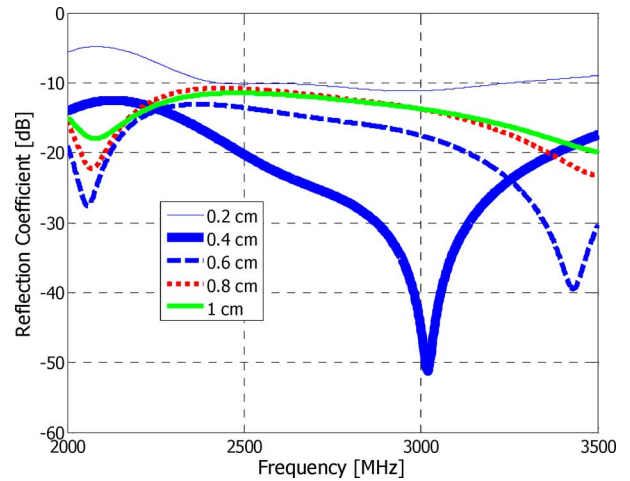


Fig. 6. Bottom fed antenna reflection coefficient through a sweep of the antenna height above the ground plane.

The shape and dimensions of the ground plane for the bottom fed antenna are optimized using simulations. A circular ground plane, with a diameter that is equal to the height of the antenna, is shown to be a good solution to preserve the properties of a conical log spiral antenna. The height of the antenna above the ground plane also plays a role in the antenna matching, as summarized in Fig. 6. This plot corresponds to five values between 0.2 and 1 cm.

The axial ratio for the bottom fed conical log spiral antenna at  $f = 2.2, 2.4, 2.6,$  and  $2.8$  GHz is summarized in Fig. 7 for both  $\Phi = 0^\circ$  and  $90^\circ$  planes. The axial ratio is plotted for a span of theta angles from  $0^\circ$  to  $180^\circ$ . A symmetrical plot can be obtained for the other span of theta angles from  $0^\circ$  to  $-180^\circ$ . An axial ratio below 3 dB is obtained within a specific range of theta angles for each operating frequency. This range depends on the operating beamwidth of the conical log spiral antenna at each frequency. It is essential to note that the axial ratio at  $f = 2.2$  GHz is above 3 dB. This is postulated to be an artifact of the feeding system since it is modeled within the simulator as large horizontal lines. This is solved in the fabricated prototype that is fed by an appropriate feeding network as discussed in the following sections.

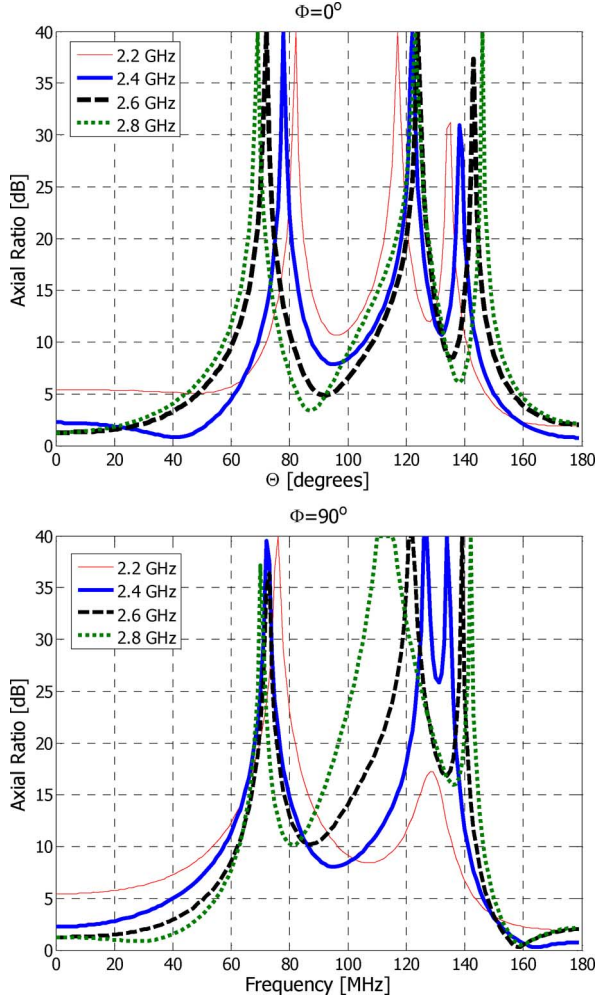


Fig. 7. Axial ratio for the bottom fed conical log spiral antenna in both the  $\phi = 0^\circ$  and  $90^\circ$  planes for a set of different frequencies.

Based on the results detailed in this section, we came up to the conclusion that a conical log spiral antenna fed at its apex has almost the same radiation characteristics as a bottom fed one. However, a circular ground plane should be included whose diameter should be comparable to the height of the antenna.

### III. FEEDING NETWORK OF THE BOTTOM FED CONICAL LOG SPIRAL ANTENNA

Like all antennas that need differential feeds, the input must be balanced and  $180^\circ$  out of phase in order to achieve the specified input match and radiation characteristics [12]. For the conical log spiral, it must be noted that any deformation of the radiation pattern can be traced back to the input feed [2].

The proposed feeding network is summarized in Fig. 8(a). It is printed on Rogers 4003 with a dielectric constant of 3.38 and a height of 0.4 mm. The input (port 1) is a  $50\ \Omega$  microstrip line that is connected to the input of a commercial balun [13]. The balun achieves a different impedance split as well as an  $180^\circ$  phase difference. The two outputs of the balun (ports 2&3) have an impedance of  $25\ \Omega$ . Each output port is fed to a quarter wavelength transformer (QWT) to provide the appropriate matching.

Authorized licensed use limited to: American University of Beirut. Downloaded on April 17, 2024 at 06:57:14 UTC from IEEE Xplore. Restrictions apply.

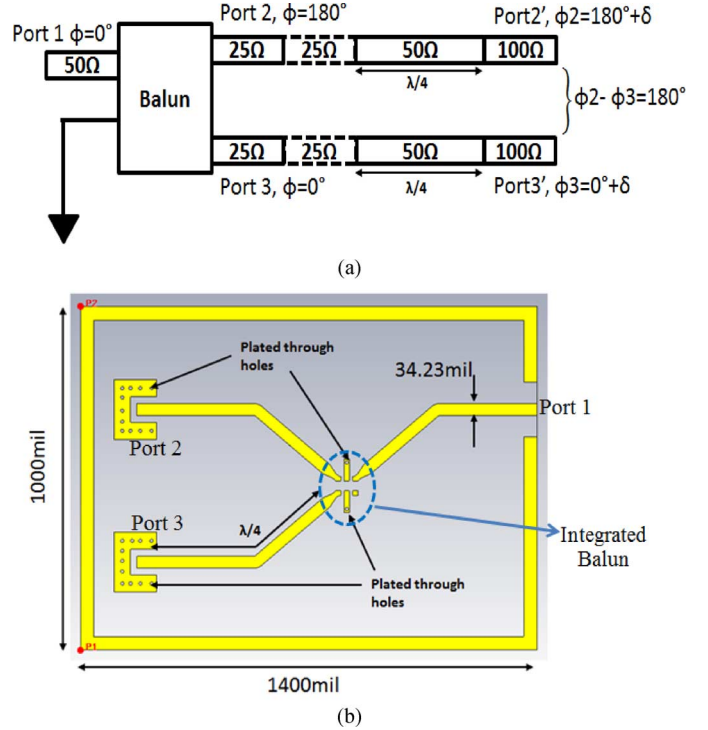


Fig. 8. (a) Feeding network circuit diagram and (b) the physical layout of the feeding network.

The proposed bottom fed conical log spiral antenna has a differential input impedance of  $200\ \Omega$ . Therefore, the QWT transforms the output impedance of the balun to  $100\ \Omega$  on each arm. This will achieve a differential impedance of  $200\ \Omega$  between the two output ports of the QWT is preserved since equal length lines are used.

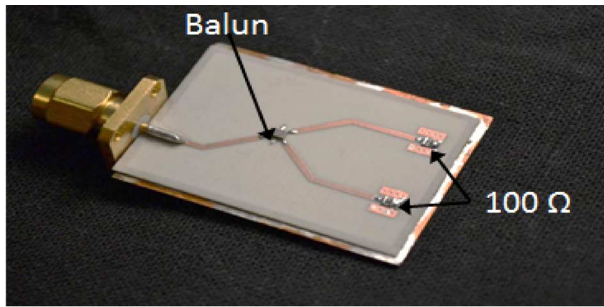
The physical layout of the feeding network circuit is shown in Fig. 8(b). The layout for the integrated balun is taken from the suggested layout located within the data sheet [13]. The used balun has six pins: two pins are connected to the ground through “vias”, one pin is connected to port 1, and two others to port 2 and 3, and the last pin is left unconnected.

To test the proposed feeding network, two  $100\ \Omega$  resistors are connected at the end of the two output ports (port 2 and 3) as shown in Fig. 9(a). To feed the two arms of the bottom fed conical log spiral antenna, the two  $100\ \Omega$  resistors are replaced by  $100\ \Omega$  coaxial cables as summarized in Fig. 9(b).

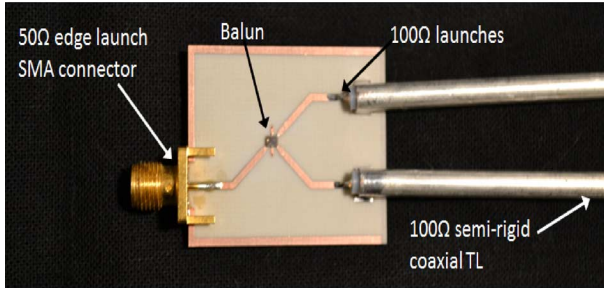
The comparison between the simulated and measured reflection coefficient of the feeding network is shown in Fig. 10. A good agreement is obtained between both data. It is essential to note that the obtained operating bandwidth for the feeding network is little bit narrower than the bottom fed conical log spiral antenna discussed in the previous section.

### IV. ANTENNA AND FEED ASSEMBLY

The output ports 2 and 3 of the feeding network are connected to Micro-Coax  $100\ \Omega$  lines. These lines are used as launchers from the balun to the arms of the bottom fed conical log spiral. The fabrication of such an antenna requires ultimate accuracy in achieving the exact rate of change in width spacing and length.



(a)



(b)

Fig. 9. (a) Fabricated feeding network terminated by  $100\ \Omega$  resistors at the two output ports and (b) the feeding network with the coaxial transmission lines at the two output ports.

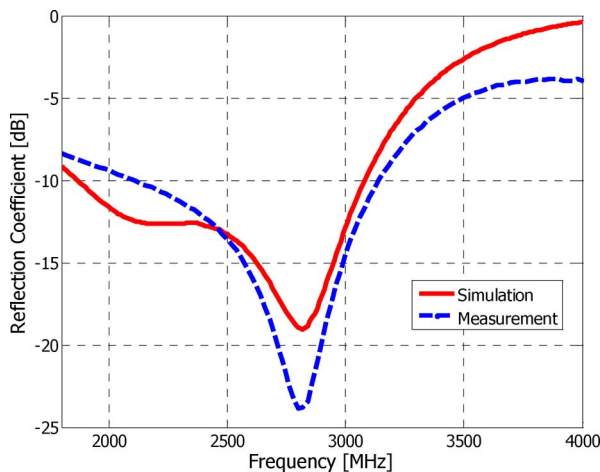


Fig. 10. Simulated and measured reflection coefficient of the feeding network.

Therefore the two arms have to be flattened into a planar pattern by dropping the  $z$ -component from the design equations. The spiral pattern is then printed and removed from a copper sheet.

After the etching is completed, the antenna arms are then wrapped around a foam cone that has the same volumetric dimensions as the simulated inner cone composing the antenna. The cone only plays a support role for the arms that are now wrapped around it. It is composed of foam with a dielectric constant  $\epsilon_r = 1$ .

A ground plane is created using a solid sheet of thick copper that is cut into a circular form with the diameter equals the height of the antenna. The antenna is deployed above the ground plane. The distance between the antenna and the ground is optimized

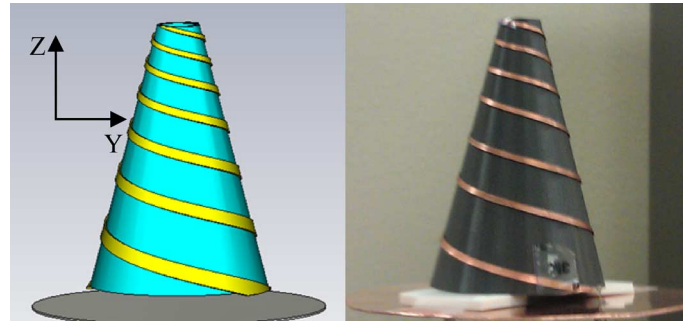


Fig. 11. Comparison of the simulation (left) and constructed (right) bottom fed conical log spiral antenna.

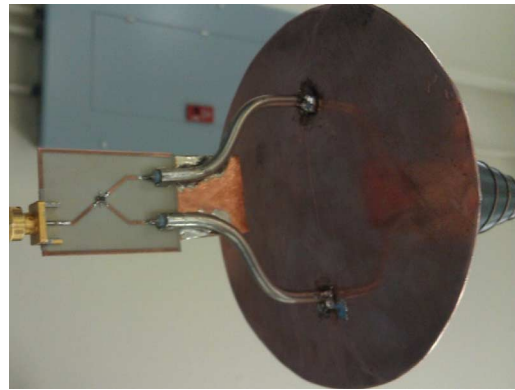


Fig. 12. Feeding network attached to the antenna.

using simulation for a better performance, as mentioned previously. The fabricated antenna is compared to the simulated one in Fig. 11.

## V. RESULTS

The connection from the feeding network to the antenna arms is achieved as shown in Fig. 12. The semi-rigid coaxial lines are inserted through the antenna's ground plane where holes are drilled. The center conductors of the coaxial lines are soldered to the antenna arms and the outer conductors are soldered to the ground plane of the antenna.

The antenna's input reflection coefficient is measured, where the input of the feeding system is connected for a single port measurement on the network analyzer. The measured reflection coefficient of the antenna attached to the feeding network is shown in Fig. 13. The total bandwidth of the antenna is measured to be 2.2–3.1 GHz, which is directly affected by the bandwidth of the balun in the feeding network.

Comparing the simulated and measured patterns, it can be seen that the main beam is consistent, while there is a reduction in the measured back lobes as shown in Fig. 14. This is due to the practical influences of the feed system during measurements. This doesn't exist in simulations since the feeding network is assumed to be ideal.

The peak gain of the two cross polarizations (V: Vertical, H: Horizontal) for the bottom fed conical log spiral antenna are measured using a standard linearly polarized horn antenna [14]. The simulated and measured gain for the span of frequency from

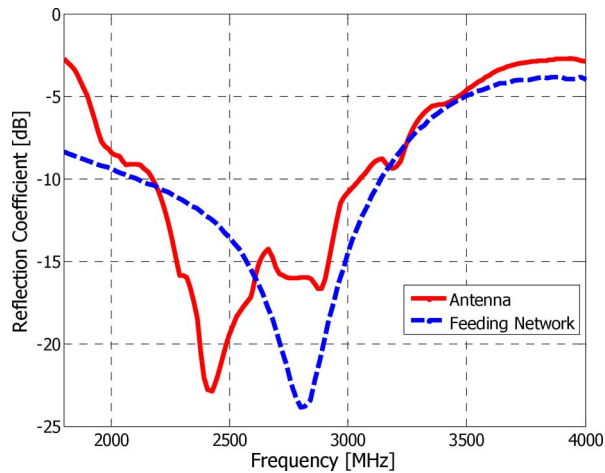


Fig. 13. Measured reflection coefficient of the “antenna connected to the feeding network” versus the feeding network alone.

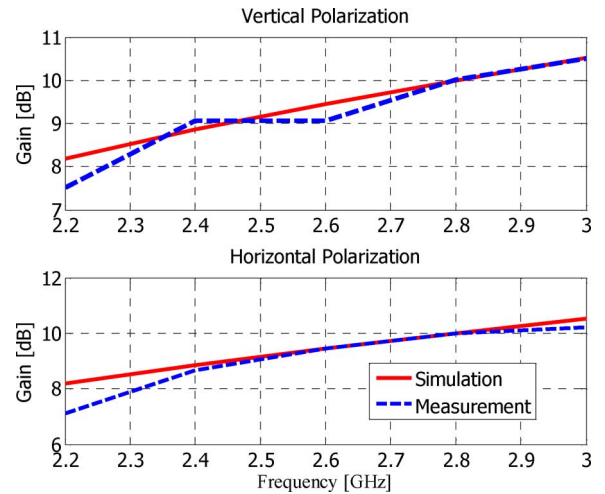


Fig. 15. Simulated and measured antenna gain for both polarizations.

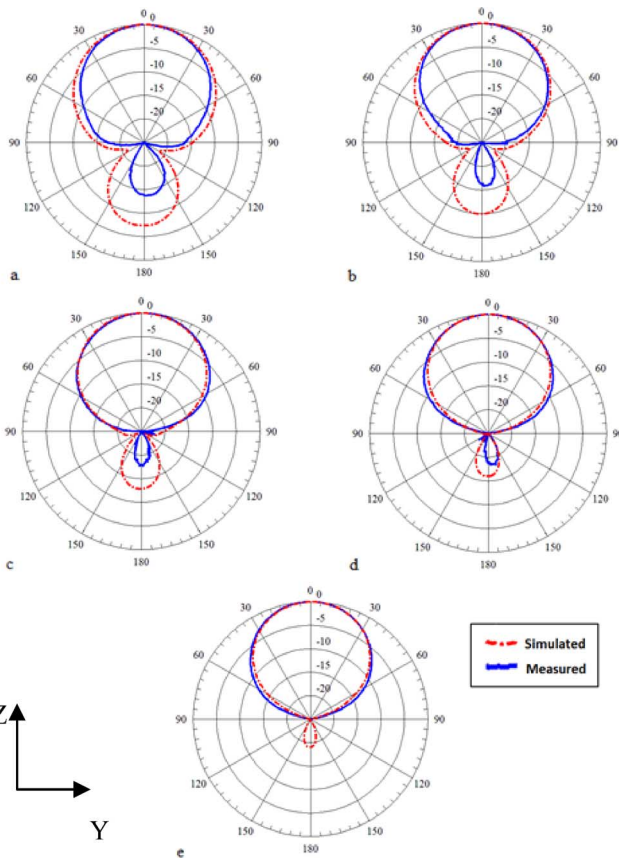


Fig. 14. Simulated and measured patterns in the  $Y-Z$  plane for different frequencies. (a) 2.2 GHz. (b) 2.4 GHz. (c) 2.6 GHz. (d) 2.8 GHz. (e) 3.0 GHz.

2.2 to 3 GHz is plotted in Fig. 15. The gain values of the measured antenna, for both polarizations, are found to be approximately the same value as the simulated ones. The measured axial ratio in the  $\Phi = 90^\circ$  plane at  $f = 2.2$  and 2.8 GHz for the span of theta angle from  $0^\circ$  to  $180^\circ$  is summarized in Fig. 16. The antenna is able to produce circularly polarized waves for  $0^\circ < \theta < +55^\circ$  at  $f = 2.2$  GHz and  $0^\circ < \theta < 41^\circ$  at  $f = 2.8$  GHz since the axial ratio is below 3 dB along these angles. The same

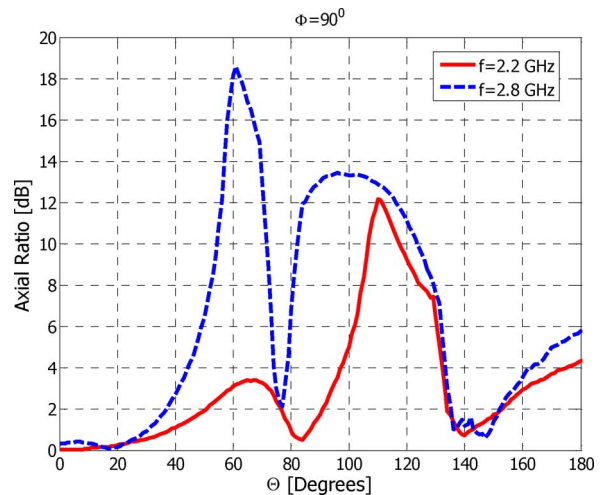


Fig. 16. Measured antenna axial ratio at  $f = 2.2$  and 2.8 GHz in the  $\Phi = 90^\circ$  plane.

axial ratio values can be obtained for  $-55^\circ < \theta < 0^\circ$  at  $f = 2.2$  GHz and  $-41^\circ < \theta < 0^\circ$  at  $f = 2.8$  GHz. This is expected since the antenna beamwidth lies within this span of angles.

## VI. CONCLUSION

In this paper, a bottom fed conical log spiral antenna is discussed. It is found that this technique is successful if the antenna is deployed on top of a ground plane. The ground plane dimensions have to be optimized to satisfy the design constraints and improve the antenna's radiation characteristics.

A comparison between the measurements and simulations of the bottom fed conical log spiral antenna shows great analogy. Thus, this paper proves that a bottom fed conical log spiral antenna constitutes a potential antenna candidate for CubeSat or any other Satellite platform. Its ability to be bottom fed with a deployable ground plane preserves the same characteristics of a top fed conical log spiral antenna with an easier deployment mechanism.

## REFERENCES

- [1] R. Nugent, R. Munakata, A. Chin, R. Coelho, and J. PuigSuari, "The CubeSat: The picosatellite standard for research and education," presented at the Amer. Inst. Astronaut. Astronaut. SPACE Conf. Expo., San Diego, CA, USA, Sep. 2008.
- [2] T. Tadashi, K. Miura, M. Natori, E. Hanayama, T. Inoue, T. Noguchi, N. Miyahara, and H. Nakaguro, "Deployable antenna with 10-m maximum diameter for space use," *IEEE Trans. Antennas Propag.*, vol. 52, no. 1, pp. 2–11, Jan. 2004.
- [3] J. Winter, G. Spanjers, D. Cohen, A. Adler, G. Ginet, B. Dichter, J. Granata, K. Denoyer, T. Murphey, P. Wegner, L. Underwood, P. Hausgen, and D. Senft, "A proposed large deployable space structures experiment for high power, large aperture missions in MEO," in *Proc. IEEE Aerosp. Conf.*, Mar. 2004, vol. 1, pp. 525–532.
- [4] F. Zheng, M. Chen, W. Li, and P. Yang, "Conceptual design of a new huge deployable antenna structure for space application," in *Proc. IEEE Aerosp. Conf.*, 2008, pp. 1–7.
- [5] T. W. Murphey and S. Pellegrino, "A novel actuated composite tape-spring for deployable structures," AIAA, Palm Springs, CA, USA, Tech. Rep. TR-1528, 2004.
- [6] S. Jeon and T. W. Murphey, "Design and analysis of a meter-class CubeSat boom with a motor-less deployment by bi-stable tape springs," presented at the 52nd AIAA Structures, Structural Dyn., Mater. Conf., Denver, CO, USA, Apr. 2011.
- [7] T. W. Murphey, S. Jeon, A. Biskner, and G. Sanford, "Deployable booms and antennas using bi-stable tape-springs," presented at the 24th AIAA/SU Conf. Small Satellites, Logan, UT, USA, 2010.
- [8] J. Costantine, Y. Tawk, C. G. Christodoulou, J. Banik, and S. Lane, "CubeSat deployable antenna using bistable composite tape-springs," *IEEE Antennas Wireless Propag. Lett.*, vol. 11, pp. 285–288, 2012.
- [9] J. Dyson, "The characteristics and design of the conical log-spiral antenna," *IEEE Trans. Antennas Propag.*, vol. AP-13, no. 4, pp. 488–499, Jul. 1965.
- [10] T. Milligan, *Modern Antenna Design*, 2nd ed. New York, NY, USA: Wiley-IEEE Press, 2005.
- [11] J. Costantine, Y. Tawk, A. Ernest, and C. G. Christodoulou, "Deployable antennas for CubeSat and space communications," in *Proc. 6th Euro. Conf. Antennas Propag.*, 2012, pp. 837–840.
- [12] K. Ang and Y. Leong, "Converting baluns into broad-band impedance-transforming 180° hybrids," *IEEE Trans. Microwave Theory Techn.*, vol. 50, no. 1, pp. 228–230, Aug. 2002.
- [13] Anaren, East Syracuse, NY, USA, "Ultra low profile 805 Balun 50  $\Omega$  to 50  $\Omega$  balanced," Model BD2130J5050AHF Data Sheet, 2014.
- [14] C. A. Balanis, *Antenna Theory Analysis and Design*, 3rd ed. Hoboken, NJ, USA: Wiley, 2005.

**Anthony J. Ernest** received the B.S.E.E. and M.S.E.E. degrees from The University of New Mexico, Albuquerque, NM, USA, in 2010 and 2012, respectively.

He is currently a member of the technical staff at Sandia National Laboratories, Albuquerque, NM, USA. He is currently working with the design and manufacturing of custom UHF–Ku-Band RF/microwave elements ranging from distributed elements and active devices to antenna design.



**Youssef Tawk** received the bachelor's degree in computer and communication engineering (highest distinction) from Notre Dame University, Louaize, Lebanon, in 2006, the master's degree in electrical and computer engineering from the American University of Beirut, Beirut, Lebanon, in 2008, and the Ph.D. degree from the University of New Mexico, Albuquerque, NM, USA, in 2011, where he also completed a post-doc fellowship, in August 2012.

He has published several journal and conference papers and has several issued patents. His research interests include cognitive radio, reconfigurable antenna systems, deployable antennas and millimeter-wave technology.

Dr. Tawk was a recipient of many awards and honors throughout his studies.



**Joseph Costantine** received the bachelor's degree in electrical, electronics, computer, and communications engineering from the second branch of the Faculty of Engineering, Lebanese University, Beirut, Lebanon, in 2004, the master's degree in computer and communications engineering from the American University of Beirut, Beirut, Lebanon, in 2006, and the Ph.D. degree from the University of New Mexico, Albuquerque, NM, USA, in 2009, where he also completed a post-doc fellowship in July 2010.

He has published many research papers and has several patents. His major research interests reside in reconfigurable antennas for wireless communication systems, cognitive radio, antennas for biomedical applications and deployable antennas for small satellites.

Dr. Costantine was a recipient of many awards including the summer faculty fellowship from the space vehicles directorate in Albuquerque, NM, for three consecutive years.



**Christos G. Christodoulou** (F'02) received the Ph.D. degree in electrical engineering from North Carolina State University, Raleigh, NC, USA, in 1985.

He served as a faculty member in the University of Central Florida, Orlando, from 1985 to 1998. In 1999, he joined the faculty of the Electrical and Computer Engineering Department, University of New Mexico, where he served as the Chair of the Department from 1999 to 2005. He is a Distinguished Professor at UNM. Currently, he is the

Associate Dean of Research for the School of Engineering at UNM, and served as the director for COSMIAC (Configurable Space Microsystems Innovations & Applications Center) at UNM. He served as the major advisor for 25 Ph.D. and 70 M.S. students. He has published about 500 papers in journals and conferences, has 14 book chapters, and has co-authored 6 books. His research interests include the areas of modeling of electromagnetic systems, cognitive radio, machine learning in electromagnetics, high power microwave antennas, and reconfigurable antennas for cognitive radio.

Dr. Christodoulou is the Chair for the APS Awards and Fellows Committee. He was appointed as an IEEE AP-S Distinguished Lecturer (2007–2010) and elected as the President for the Albuquerque IEEE Section in 2008. He served as an associate editor for the IEEE TRANSACTIONS ON ANTENNAS AND PROPAGATION for six years, as a guest editor for a special issue on "Applications of Neural Networks in Electromagnetics" in the *Applied Computational Electromagnetics Society (ACES) Journal*, and as the co-editor of a the IEEE TRANSACTIONS ON ANTENNAS AND PROPAGATION special issue on "Synthesis and Optimization Techniques in Electromagnetics and Antenna System Design" (March 2007). He was a recipient of the 2010 IEEE John Krauss Antenna Award for his work on reconfigurable fractal antennas using MEMS switches, the Lawton-Ellis Award, and the Gardner Zemke Professorship at the University of New Mexico. He is a member of Commission B of URSI.